

Article

Joint Task Allocation and Resource Optimization Based on an Integrated Radar and Communication Multi-UAV System

Xun Zhang ^{1,*}, Kehao Wang ^{1,*} , Xiaobai Li ², Kezhong Liu ³ and Yirui Cong ⁴

¹ School of Information Engineering, Wuhan University of Technology, Wuhan 430070, China; xun.zhang@whut.edu.cn

² Department of Early Warning Intelligence, Air Force Early Warning Academy, Wuhan 430070, China; lxb2cici@163.com

³ School of Navigation, Wuhan University of Technology, Wuhan 430070, China; kzliu@whut.edu.cn

⁴ College of Intelligence Science and Technology, National University of Defense Technology, Changsha 410073, China; congyirui11@nudt.edu.cn

* Correspondence: kehao.wang@whut.edu.cn

Abstract: This paper investigates the joint task allocation and resource optimization problem in an integrated radar and communication multi-UAV (IRCU) system. Specifically, we assign reconnaissance UAVs and communication UAVs to perform the detection, tracking and communication tasks under the resource, priority and timing constraints by optimizing task allocation, power as well as channel bandwidth. Due to complex coupling among task allocation and resource optimization, the considered problem is proved to be non-convex. To solve the considered problem, we present a loop iterative optimization (LIO) algorithm to obtain the optimal solution. In fact, the mentioned problem is decomposed into three sub-problems, such as task allocation, power optimization and channel bandwidth optimization. At the same time, these three problems are solved by the divide-and-conquer algorithm, the successive convex approximation (SCA) algorithm and the improved particle swarm optimization (PSO) algorithm, respectively. Finally, numerical simulations demonstrate that the proposed LIO algorithm consumes fewer iterations or achieves higher maximum joint performance than other baseline schemes for solving the considered problem.

Keywords: IRCU system; task allocation; power; channel bandwidth; LIO algorithm



Citation: Zhang, X.; Wang, K.; Li, X.; Liu, K.; Cong, Y. Joint Task Allocation and Resource Optimization Based on an Integrated Radar and Communication Multi-UAV System. *Drones* **2023**, *7*, 523. <https://doi.org/10.3390/drones7080523>

Academic Editor: Emmanouel T. Michailidis

Received: 30 May 2023

Revised: 26 July 2023

Accepted: 2 August 2023

Published: 10 August 2023



Copyright: © 2023 by the authors. Licensee MDPI, Basel, Switzerland. This article is an open access article distributed under the terms and conditions of the Creative Commons Attribution (CC BY) license (<https://creativecommons.org/licenses/by/4.0/>).

1. Introduction

Due to their flexible on-demand deployment, high mobility [1] and free trajectory design [2], unmanned aerial vehicles (UAVs) are considered to be an important component for the future battlefield, providing both ubiquitous communication and radar sensing capabilities [3]. For emergency situations, such as disaster relief or on the battlefield, UAVs can not only detect and track enemy targets to avoid the potential attack [4], but also provide instant communication to the command center [5].

Although the advantages of a single UAV for detection or tracking [6,7] have been demonstrated, its capabilities are generally limited by resource and quantity constraints, and it may not be able to meet the communication requirements [8]. Additionally, in single-site positioning, multiple distance measurements of the same target by a single UAV may lead to large cumulative errors [9]. Moreover, UAV-assisted IoT systems are proven worthy of integration in the next generation of wireless protocols, but there are issues of signal quality loss and spectrum constraints in real-world implementation [10–12]. And these problems can potentially be overcome by a multi-UAV system. Recently, many scholars have applied multi-UAVs to perform complex tasks, for example, in the literature [13–19]. In [13], the authors proposed a method for cooperative multi-UAV reconnaissance task planning in a denied environment based on an improved synthetic heuristic algorithm, which was used to solve the problem that the traditional intelligent algorithm could not

meet the requirements for cooperative multi-UAV reconnaissance task planning due to slow convergence and the tendency to fall into local optima. The authors of [14] proposed an improved K-means clustering analysis algorithm to solve the problem of too many reconnaissance targets for UAV applications in the battlefield environment. In [15], an UAV, an unmanned surface vehicle (USA) and an autonomous underwater vehicle (AUV) were combined to implement a search-and-track (SAT) mission for an underwater target, and strategies based on random simulation experiments and asynchronous planning were developed to design the cooperative path planning algorithm in the search track phases. To solve the problem of poor timeliness and large communication volume in the traditional contract network protocol (CNP) when dealing with the dynamic multi-UAV cooperative reconnaissance task assignment problem, an improved contract network protocol was proposed in [16]. To address the problem of a high tracking success rate that is difficult to be satisfied by a single UAV, a deep reinforcement learning (DRL) algorithm was designed to allow UAVs to make intelligent flight action decisions to track the moving air target in [17]. To solve the problem of the poor solution accuracy when using the GA algorithm for large-scale task assignment of UAVs, a new algorithm combining reinforcement learning and GA algorithm was proposed in [18]. The authors in [19] presented a new approach to route planning for joint search and track missions by coordinated UAVs. From the above literature, it is clear that they only consider multi-UAVs performing reconnaissance and tracking tasks on the battlefield using radar, and do not consider communication tasks where the UAVs gather targets' information and transmit the information to the command center. However, the deployment of a large number of UAVs, some providing communication services and others performing radar sensing, will not only introduce co-channel interference between the communication and radar systems, but also increase the resource consumption.

To deal with these above problems, an integrated radar and communication (IRC) [20–26] can be considered as a potential solution. In IRC, most of the hardware and signal processing is shared between communication and radar due to the sharing of a common transmission signal. As a result, the use of the payload and resources can be minimized. To enable communication links by controlling the transmit beamforming, a dual-function system with joint radar and communication platforms was developed in [20]. The authors in [21] proposed the use of a single transmitter with multiple antennas to communicate with downlink cellular users and simultaneously detect the targets. To trade off the performance between radar and communication, the authors in [22] proposed an IRC MIMO system, which minimized the downlink multi-user interference under a constant modulus constraint and a similarity constraint on the referenced radar signals. To ensure the downlink communication performance of the IRC system, the authors in [23] developed a beam pattern to enhance the radar sensing performance. To overcome the typical drawbacks of radar processing, the authors designed an OFDM system for simultaneous radar and communication operations in [24]. The authors in [25] proposed a novel multibeam framework that allows seamless integration of communication and sensing. In [26], closed-form solutions for optimizing the coefficients in the analogue antenna arrays were developed, which generated a multibeam for joint communication and radio sensing.

By taking advantage of multi-UAVs and IRC systems, it is possible to improve the performance of communication and radar sensing with reduced resource consumption. There has been little work aimed at using the IRC multi-UAV (IRCU) system to perform complex tasks [27–30]. In [27], the authors studied the cooperative UAV sensing in multi-UAV networks, specifically, UAVs equipped with sensors, communication, and computational units to sense the environment by performing surveillance and computational tasks. The authors in [28] proposed a cyber-twin-based distributed tracking algorithm to solve the problem of realizing low-overhead UAV swarm cooperation to track multi-targets in a distributed architecture. The authors in [29,30] proposed a novel multi-UAV cooperative sensing and communication scheme with overlapped sensing task allocation by taking full advantage of multi-UAV sensing and communication.

However, the above literature basically considers sensors to sense the environment rather than using radar to detect and track targets. Therefore, a number of important issues need to be addressed, such as task allocation, transmission power allocated to each UAV, channel bandwidth allocated to each sub-channel for each communication task. In this paper, we study an IRCU system, where multiple UAVs are employed to cooperatively detect and track the targets and simultaneously transmit the collected information to the command center.

Therefore, the purpose of this paper is to study a joint task allocation and resource optimization problem in the IRCU system under the resource, priority and timing constraints. The main contributions are summed up as follow:

- We consider a joint task allocation and resource optimization problem in the IRCU system under the resource, priority and timing constraints by jointly optimizing task allocation, power as well as channel bandwidth, and formulate the considered problem.
- Considering the mentioned complex non-convex problem, we propose an LIO algorithm, which obtains the optimal solution in a loop iterative manner.
- The considered problem is actually decomposed into three sub-problems, such as task allocation, power optimization and channel bandwidth optimization. At the same time, these three problems are solved by the divide-and-conquer algorithm, the SCA algorithm and the improved PSO algorithm, respectively.
- Simulation results demonstrate that the LIO algorithm consumes fewer iterations or gains higher maximum joint performance than other baseline schemes for solving the considered problem.

The rest of this paper is organized as follows. Section 2 depicts the joint task allocation and resource optimization problem in the IRCU system under the resource, priority and timing constraints with its mathematical formulation. In Section 3, we decompose the considered problem into three sub-problems, and propose an LIO algorithm for solving the corresponding problem in a loop iterative manner. Section 4 conducts several simulations and comparisons to verify the feasibility and effectiveness of the proposed algorithm. This paper is concluded in Section 5.

2. System Model and Problem Formulation

The main parameters of this paper is shown in Table 1.

Table 1. Simulation parameter settings.

Variables	Explanation
N	The number of tasks
N_1	The number of communication tasks
N_t	The number of task types
M	The number of UAVs
\mathcal{N}	The task set
\mathcal{M}	The UAV set
H	The hovering altitude of the large flying platform
T_{total}	The total time
P_{total}	The total power
B_{total}	The total channel bandwidth
i	The task index
j	The task type
s_i	The task type to which the i -th task belongs
$P_{r,i}$	The importance level of task i
$T_{d,i}$	The deadline time of task i
$T_{c,i}$	The dwell time of task i
T_i	The return time of task i
R_i	The designated distance of task i
p_i	The consumption power of task i
B_i	The channel bandwidth of task i

Table 1. Cont.

Variables	Explanation
$f(s_i)$	a 0–1 decision function
\mathbf{S}	The task type matrix
\mathbf{P}	The task consumption power vector
\mathbf{B}	The channel bandwidth vector
\mathbf{F}	The task allocation matrix
\mathbf{Q}	The observation noise covariance
t_{SI}	The scheduling interval
$R_{i,j}$	The task performance of task i that belongs to task type j
$P_{\min,j}$	The minimum task performance of task type j
P_{\min}	The mainimum power
P_{\max}	The maximum power
B_{\min}	The mainimum channel bandwidth
B_{\max}	The maximum channel bandwidth
p_{fa}	The false alarm probability of the receiver
h_0	The channel gain of the line-of-sight channel
N_0	The power spectral density of noise
P_h	The power consumed by each UAV while hovering
γ	The minimum task scheduling success rate
w_j	The weight coefficient of the j -th task type

2.1. System Model

As shown in Figure 1, we consider an IRCU system where the reconnaissance UAVs detect and track the targets, and then the communication relay UAVs trasmit their collected information to their corresponding communication nodes. There exists N tasks, the set of which is denoted by $\mathcal{N} = \{1, 2, \dots, N\}$. The set of M UAVs, denoted by $\mathcal{M} = \{1, 2, \dots, M\}$, consists of reconnaissance UAVs and communication relay UAVs, which are all grouped together on a large flying platform. In this system, we make some assumptions as follows: (1) The platform is hovering at $\mathbf{X}_0 = [0, 0, H]$; (2) The different types of UAVs all take off from the platform and fly to the designated task site to perform tasks; (3) Since the topic of this paper focuses on the process on the process of UAV task execution, the resource consumption of platform hovering and UAV flying to the task location is ignored; (4) The UAVs in this platform are assigned to perform the detection, tracking and communication tasks independently, i.e., each UAV only selects one task, and the corresponding type of UAVs is needed to perform the corresponding task of the IRCU system, e.g., reconnaissance UAVs perform detection and tracking tasks, and so on; (5) The UAV arrives at the designated task site, hovers and performs its task; (6) The time interval between two consecutive scheduling of the same task is defined as the return time. Note that these tasks are not executed in a specific sequence. Thus, we consider the task scheduling problem of the IRCU system that is aiming at the scheduling of UAVs.

We define N_t as the number of task types, where N_t is equal to 3 and the task types are detection, tracking and communication, respectively. Let $\mathbf{S} = [s_i]_{1 \times N}$ be a task type marix where s_i denotes the type of task to which the i -th task belongs. We assume that the i -th task of the integrated UAV task scheduling is defined as $\mathcal{T}_i = \{P_{r,i}, T_{d,i}, T_{c,i}, T_i, R_i\}$, where $P_{r,i}$ is the importance level of the i -th task; $T_{d,i}$ is the deadline time of the i -th task; $T_{c,i}$ and T_i are the dwell time and the return time of the i -th task; R_i is the designated distance of the i -th task. Define $\mathbf{P} = [p_1, p_2, \dots, p_N]$ and $\mathbf{B} = [B_1, B_2, \dots, B_{N_1}]$ be the task consumption power vector and the channel bandwidth vector, respectively, where N_1 is the number of communication tasks. Note that a scheduling interval T_{SI} is the maximum return time among N tasks.

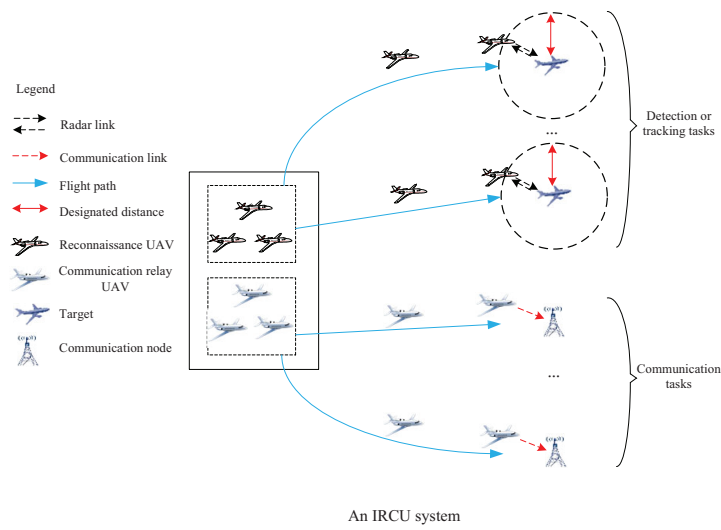


Figure 1. An IRCU system.

2.2. Task Model

The task analysis of the IRCU system includes three main components: detection, tracking and communication.

2.2.1. Detection

Assume that Swerling type I target is considered. If the i -th task is the detection task and the radar of each UAV transmits a pulse, the detection probability of single pulse transmitted by the reconnaissance UAV is [31]

$$p_{d,i} = (1 + \mu_{d,i}) \sqrt{p_{fa}} \tag{1}$$

where p_{fa} is the false alarm probability of the receiver; $\mu_{d,i}$ is the return signal-to-noise ratio (SNR) of the radar receiver. When p_{fa} is a constant, $p_{d,i}$ is only determined by $\mu_{d,i}$.

For ease of calculation, we define

$$R_{i,1} = p_{d,i} \tag{2}$$

which satisfies

$$R_{i,1} \geq P_{\min,1} \tag{3}$$

where $P_{\min,1}$ is the minimum probability that the i -th task is successfully scheduled.

Referring to [32], $\mu_{d,i}$ is written as

$$\mu_{d,i} = \frac{p_i A_r \sigma_d T_{c,i}}{4\pi k_B L_s T_e R_i^4 \theta} \tag{4}$$

where p_i is the average transmitter power of the radar of the reconnaissance UAV when performing task i ; A_r denotes the effective receiving antenna area; σ_d represents the radar cross section of the target; L_s is the system loss; k_B denotes Boltzmann parameter; T_e represents the system temperature; R_i denotes the designated distance of radar detection when performing task i ; θ represents the research angle. Let

$$\alpha = \frac{A_r \sigma_d}{4\pi k_B L_s T_e \theta} \tag{5}$$

we can rewrite (5) compactly as follows

$$\mu_{d,i} = \frac{\alpha p_i T_{c,i}}{R_i^4} \tag{6}$$

2.2.2. Tracking

If the i -th task is the tracking task, the observation noise covariance \mathbf{Q} of the radar in performing target tracking can be expressed as

$$\mathbf{Q} = \begin{bmatrix} \sigma_\phi^2 & 0 \\ 0 & \sigma_\phi^2 \end{bmatrix} = \begin{bmatrix} \sigma_\phi(T_i)^2 & 0 \\ 0 & \sigma_\phi(\mu_{t,i})^2 \end{bmatrix} \quad (7)$$

where σ_ϕ^2 is the distance measurement error value, which is mainly associated with T_i ; σ_ϕ^2 denotes the angular measurement error value, which is mainly associated with $\mu_{t,i}$. And the mathematical expression of the angular measurement error is [33]

$$\sigma_{\phi_i} = \theta_{\text{dB}} / (K_m \sqrt{2\mu_{t,i}}) \quad (8)$$

where θ_{dB} is the width of the radar antenna beam; K_m is a constant; $\mu_{t,i}$ is the radar echo signal-to-noise ratio of task i , which is defined as [33]

$$\mu_{t,i} = \frac{p_i \sigma_t L_r T_{c,i}}{R_i^4} \quad (9)$$

where p_i is the radar transmitting power of the reconnaissance UAV when performing task i ; σ_t is the tracked target cross-sectional area; L_r is the radar constant of the reconnaissance UAV; R_i is the designated distance of radar tracking when performing task i .

When the reconnaissance UAV is tracking a target, the target tracking accuracy is related to the observation noise covariance \mathbf{Q} . Since T_i is given, the target tracking accuracy is mainly related to $\mu_{t,i}$. Thus, the IRCU system takes the angular error value as the tracking accuracy and the radar echo signal-to-noise ratio as a metric. Then, the target tracking accuracy is written as

$$R_{i,2} = \mu_{t,i} \quad (10)$$

which satisfies

$$R_{i,2} \geq P_{\min,2} \quad (11)$$

where $P_{\min,2}$ is the minimum radar echo signal-to-noise ratio.

2.2.3. Communication

If the i -th task is the communication task, the communication relay UAV of the IRCU system communicates directly with the communication node on the ground. Assume that the channel between the communication relay UAV and the communication node is a line-of-sight (LOS) channel under U2U communication [34]. Thus, according to the theorem of Shannon, the transmission rate in the LOS channel model can be calculated by [35]

$$R_t = B_i \log_2 \left(1 + \frac{p_i h_0}{N_0 B_i} \right) \quad (12)$$

where p_i denotes the signal transmission power when the communication relay UAV performs task i ; h_0 is the channel gain of the LOS channel; N_0 denotes the power spectral density of noise; B_i is the channel bandwidth when performing task i .

Then, we have

$$R_{i,3} = R_t \quad (13)$$

To ensure proper communication performance, the transmission data rate of communication should be no less than the minimum transmission data rate $P_{\min,3}$ required for communication transmission, then

$$R_{i,3} \geq P_{\min,3} \quad (14)$$

2.3. Constraints

2.3.1. Task Constraint

Define $f(s_i)$ be a 0–1 decision function, and 1 means the i -task is successfully scheduled, otherwise it is unscheduled. Then,

$$f(s_i) = \begin{cases} 1, & \text{if } s_i = j \text{ and } R_{i,j} \geq P_{\min,j}, \forall i, j \\ 0, & \text{else} \end{cases} \quad (15)$$

2.3.2. Time Constraint

Define T_{Total} be the total time, and the time consumed by the IRCU system to perform tasks is

$$T_s = \sum_{i=1}^N f(s_i) \beta_i T_{c,i} \quad (16)$$

where β_i is the number of times that the i -th task is scheduled in the scheduling interval. And it satisfies

$$T_s \leq T_{\text{Total}} \quad (17)$$

2.3.3. Return Time Constraint

The return time of each task satisfies

$$T_i \leq T_{i,\max} = T_{\text{SI}} \leq T_s \quad (18)$$

2.3.4. Power Constraint

Assume that only the energy consumption of the UAV during tasks and flight is considered. Define E_{Total} be the total energy of the system, and P_h is the power consumed by each UAV when hovering, then

$$p_{\min} \leq p_i \leq p_{\max} \quad (19)$$

$$\sum_{i=1}^N f(s_i) (p_i + P_h) \leq P_{\text{total}} \quad (20)$$

2.3.5. Bandwidth Constraint

Assume that the communication relay UAV performs communication task i , the bandwidth channel satisfies

$$B_{\min} \leq B_i \leq B_{\max} \quad (21)$$

$$\sum_{i=1}^N f(s_i) B_i \leq B_{\text{total}} \quad (22)$$

2.4. Problem Formation

Considering the system resources, the number of scheduled tasks and the multi-functional constraints in the IRCU system, the joint performance of all successfully scheduled tasks of the IRCU system can be defined as

$$U(\mathbf{S}, \mathbf{P}, \mathbf{B}) = \sum_{i=1}^N \sum_{j=1}^{N_t} w_j R_{i,j} f(s_i) \quad (23)$$

where w_j is the weight coefficient of the j -th type of task.

Thus, the problem of maximizing the joint performance of all successfully scheduled tasks in the IRCU system is formulated as

$$\mathcal{P} : \max_{\mathbf{S}, \mathbf{P}, \mathbf{B}} U(\mathbf{S}, \mathbf{P}, \mathbf{B}) \quad (24)$$

$$\text{s.t.} \quad (3), (11), (14), (15), (17)–(22) \quad (25)$$

$$\sum_{i=1}^N f(s_i) \geq N\gamma \quad (26)$$

where γ is the minimum task scheduling success rate.

3. Algorithm Analysis

In this section, the problem of the maximum joint performance of all successfully scheduled tasks in the IRCU system is solved by an LIO algorithm in a loop iterative manner. Since problem \mathcal{P} is non-convex, we decompose the original problem into three sub-problems solved by the divide-and-conquer algorithm, the SCA algorithm and the improved PSO algorithm, respectively. For details, please refer to the analysis of the algorithm below.

3.1. Task Allocation

When the task-consuming power vector \mathbf{P} and the channel bandwidth vector \mathbf{B} are fixed, \mathcal{P} is rewritten as

$$\mathcal{P1} : \max_{\mathbf{S}} U(\mathbf{S}) \quad (27)$$

$$\text{s.t.} \quad (3), (11), (14), (15), (17), (18), (26) \quad (28)$$

According to the task priority of each task, the set of task types is calculated. For example, when the number of tasks $N = 3$, if the priority of 3 tasks $P_{r,1}$, $P_{r,2}$, and $P_{r,3}$ are 2.1, 1.4, and 3.1 ($P_{r,2} < P_{r,1} < P_{r,3}$), respectively, then the order of execution of the tasks is 2,1,3.

Then, define $\mathbf{F} = [f(s_i)]_{1 \times N}$ be the task allocation matrix. Thus, problem $\mathcal{P1}$ is converted to

$$\mathcal{P1}' : \max_{\mathbf{F}} U(\mathbf{F}) \quad (29)$$

$$\text{s.t.} \quad (15), (17) \sim (18), (26) \quad (30)$$

Therefore, we intend to use a divide-and-conquer algorithm to solve this sub-problem [36].

3.2. Power

When the task allocation matrix \mathbf{F} and the channel bandwidth vector \mathbf{B} are fixed, \mathcal{P} is rewritten as

$$\mathcal{P2} : \max_{\mathbf{P}} U(\mathbf{P}) \quad (31)$$

$$\text{s.t.} \quad (3), (11), (14), (19), (20) \quad (32)$$

Theorem 1. $U(\mathbf{P})$ is non-convex.

Proof. Please see Appendix A. \square

Since $U(\mathbf{P})$ is non-convex, problem $\mathcal{P2}$ is the non-convex problem. To solve the problem, SCA algorithm is adopted to achieve a sub-optimal solution of $\mathcal{P2}$. Note that

the key idea of SCA algorithm is to approximate the non-convex function to the convex function in an iterative manner [37]. For ease of calculation, (23) is written as

$$U(\mathbf{P}) = \sum_{i=1}^N \sum_{j=1}^{N_t} w_j R_{i,j}(p_i) f(s_i) \tag{33}$$

In fact, (33) can be globally lower-bounded by its first-order Taylor expansion with respect to p_i at any point [38]. Let p_i^k be the power consumed by task i at the k -th iteration, and the lower bound of $R_{i,j}$ is

$$\hat{R}_{i,j}(p_i, p_i^k) = R_{i,j}(p_i^k) + \nabla R_{i,j}(p_i^k)(p_i - p_i^k) \tag{34}$$

where $R_{i,j}(p_i^k)$ and $\nabla R_{i,j}(p_i^k)$ are the k -th task performance and the first-order derivative of $R_{i,j}(p_i^k)$ with respect to p_i^k .

Therefore, problem $\mathcal{P}2$ is approximated as the following problem

$$\mathcal{P}2' : \max_{\mathbf{P}} \sum_{i=1}^N \sum_{j=1}^{N_t} w_j \hat{R}_{i,j} f(s_i) \tag{35}$$

$$\text{s.t. } \hat{R}_{i,j} \geq P_{\min,j} \tag{36}$$

$$(19), (20) \tag{37}$$

With convex (35)–(37), $\mathcal{P}2'$ is convex. Furthermore, we can adopt the standard convex optimization techniques, such as CVX solver [11], to iteratively solve this problem. It is worth noting that the optimal solution obtained from $\mathcal{P}2'$ is a lower bound of $\mathcal{P}2$.

3.3. Channel Bandwidth

When the task allocation matrix \mathbf{F} and the task-consuming power vector \mathbf{P} are fixed, \mathcal{P} is rewritten as

$$\mathcal{P}3 : \max_{\mathbf{B}} U(\mathbf{B}) \tag{38}$$

$$\text{s.t. } (14), (21), (22) \tag{39}$$

Problem $\mathcal{P}3$ is a NP-hard problem. Since there are linear constraints and a nonlinear objective function, then $\mathcal{P}3$ is not an integer programming problem. Thus, we intend to use an intelligent algorithm to solve this sub-problem, such as PSO, GA, etc, and apply PSO to solving it.

Since PSO algorithm is prone to converge to local optimization, the sub-problem introduces the improved PSO [39]. Define $\mathbf{x} = [x_1, x_2, \dots, x_{N1}]$ and $\mathbf{v} = [v_1, v_2, \dots, v_{N1}]$ to be the position vector and the velocity vector. Note that the channel bandwidth vector \mathbf{B} is equal to \mathbf{x} . Then, when the m -th particle is at the k -th iteration, we have

$$\begin{cases} \mathbf{v}^m(k+1) = c_1 \mathbf{v}^m(k) + c_2(\mathbf{X}_1^m(k) - \mathbf{x}(k)) + c_3(\mathbf{X}_g(k) - \mathbf{x}(k)) \\ \mathbf{x}^m(k+1) = \mathbf{x}^m(k) + \mathbf{v}^m(k+1) \end{cases} \tag{40}$$

where c_1, c_2 and c_3 are learning factors; $\mathbf{X}_1^m(k)$ is the historical best position of particle m at the k -th iteration; $\mathbf{X}_g(k)$ is the historical best position of the particle population at the k -th iteration.

Then, to improve convergence speed and avoid algorithm falling into local optimization, (28) is rewritten as

$$\mathbf{v}^m(k+1) = \lambda [c_1 \mathbf{v}^m(k) + c_2(\mathbf{X}_1^m(k) - \mathbf{x}(k)) + c_3(\mathbf{X}_g(k) - \mathbf{x}(k))] \tag{41}$$

where $\lambda = \frac{1}{|8-\epsilon-\sqrt{\epsilon^2-2\epsilon}|}$, and $\epsilon = \sqrt{c_1^2 + c_2^2 + c_3^2}$. And the improved PSO is detailed in Algorithm 1.

Algorithm 1 Improved PSO Algorithm

Input: Maximum number of iterations N_k, F, P

Output: \mathbf{B}^*

- 1: Initialize the iterative index $k = 1$;
 - 2: Initialize $\mathbf{x}(k)$ and $\mathbf{v}(k)$;
 - 3: According to (40) and (41), calculate the historical best positions of individuals and group, respectively;
 - 4: **while** $k \leq N_k$ **do**
 - 5: Update $\mathbf{x}(k)$ and $\mathbf{v}(k)$ with a boundary treatment;
 - 6: According to (40) and (41), calculate and update the historical best positions of individuals and group, respectively;
 - 7: Obtain $\mathbf{B}(k) = \mathbf{x}(k)$;
 - 8: **if** $|U(\mathbf{B}(k)) - U(\mathbf{B}(k-1))| \leq \epsilon$ **then**
 - 9: Stop, obtain \mathbf{B}^* ;
 - 10: **else**
 - 11: Set $k = k + 1$, and back to step 5;
 - 12: **end if**
 - 13: **end while**
-

Therefore, the joint optimization of task allocation, power and channel bandwidth is detailed in Algorithm 2. And the mainstream flowchart for Algorithm 2 is shown in Figure 2.

Algorithm 2 Loop Iterative Optimization Algorithm

Input: $N_{\max}, \mathbf{P}^1, \mathbf{B}^1$.

Output: $\mathbf{F}^*, \mathbf{P}^*, \mathbf{B}^*$ or U^* .

- 1: Initialize the iterative index $n = 1$;
 - 2: **repeat**
 - 3: Solve $\mathcal{P}1'$ to obtain $\mathbf{F}^{n,*}$ by using the divide-and-conquer method for the given \mathbf{P}^n and \mathbf{B}^n ;
 - 4: Initialize iterative index $h = 1$;
 - 5: **repeat**
 - 6: Solve $\mathcal{P}2$ to obtain $\mathbf{P}^{n,*}$ by using SCA algorithm and CVX solver for the updated $\mathbf{F}^{n,*}$ and \mathbf{B}^n , respectively;
 - 7: **if** $\|\mathbf{P}^{h,*} - \mathbf{P}^{h-1,*}\| \leq \delta$ and $h < N_{\max1}$ **then**
 - 8: $\mathbf{P}^{n,*} = \mathbf{P}^{h,*}$;
 - 9: break;
 - 10: **end if**
 - 11: Update the iterative index $h = h + 1$;
 - 12: **until**
 - 13: **repeat**
 - 14: Solve $\mathcal{P}3$ to obtain $\mathbf{B}^{n,*}$ by using Algorithm 1 for the updated $\mathbf{F}^{n,*}$ and $\mathbf{P}^{n,*}$;
 - 15: Update the iterative index $n = n + 1$;
 - 16: Calculate $U(\mathbf{F}^n, \mathbf{P}^n, \mathbf{B}^n)$;
 - 17: **until** $n \geq N_{\max}$ or $|U(\mathbf{F}^n, \mathbf{P}^n, \mathbf{B}^n) - U(\mathbf{F}^{n-1}, \mathbf{P}^{n-1}, \mathbf{B}^{n-1})| \leq \delta$;
 - 18: Output: Optimal U^* or $\mathbf{F}^*, \mathbf{P}^*, \mathbf{B}^*$.
-

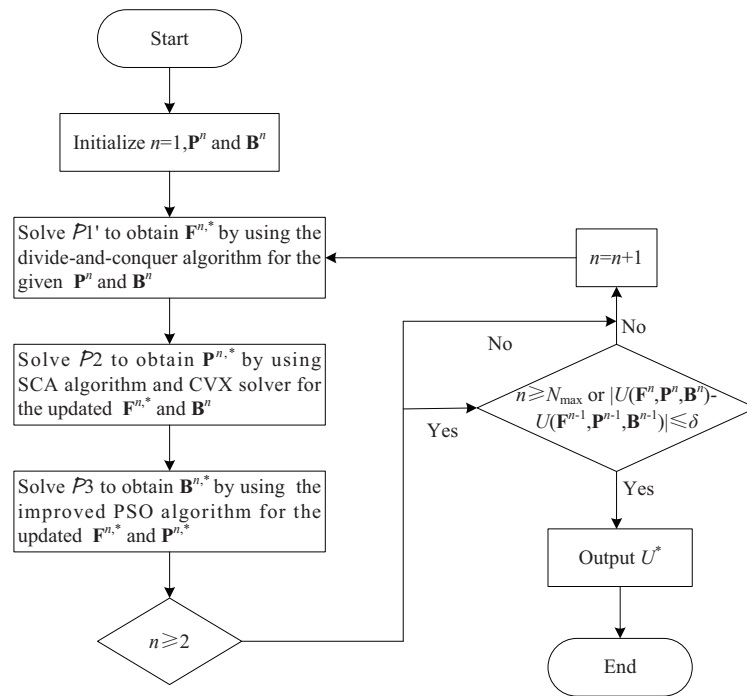


Figure 2. The mainstream flowchart for Algorithm 2.

3.4. Analysis on Convergence and Computational Complexity

In Theorem 2, the convergence of Algorithm 2 is further proved.

Theorem 2. Algorithm 2 is guaranteed to converge to the sub-optimal solution of \mathcal{P} .

Proof. Please see Appendix B. □

Moreover, the computational complexity of the proposed algorithm depends mainly on the resolution of three decomposed sub-problems. Let N be the number of tasks, N_1 denote the number of the communication tasks, K_3 denote the number of iterations of Algorithm 1, N_p represent the number of particle in Algorithm 1. Define K_1 and K_2 be the number of iterations of the outer and SCA in Algorithm 2, respectively.

For these three sub-problems, the computational complexity of the divide-and-conquer algorithm, the SCA algorithm and the improved PSO algorithm are written as, respectively,

$$C_1 = N \tag{42}$$

$$C_2 = K_2(n_1)^3 \tag{43}$$

$$C_3 = K_3N_pN_1 \tag{44}$$

where n_1 is the number of updated variables in each iteration.

Then, the computational complexity of Algorithm 2 is

$$C_t = K_1(C_1 + C_2 + C_3) \tag{45}$$

Therefore, the total computational complexity of the proposed algorithm is calculated as $\mathcal{O}(K_1(N + K_2(n_1)^3 + K_3N_pN_1))$.

4. Simulation Analysis

In this section, several simulations will be conducted to verify the proposed algorithm in the joint task allocation and resource optimization problem of the IRCU system.

To validate the effectiveness of the proposed algorithm, we compared the proposed algorithm with other baseline schemes, intelligent algorithms and Q-learning algorithm,

and applied them to the joint task allocation and resource optimization problem. The simulations were conducted in Pycharm Community's 2019.1.1 x64 version of the programming environment on an Intel Core PC with 8GB memory. The joint task performance that the IRCU earn by successfully completing N tasks is considered to be a performance metric for evaluating this system.

We consider the IRCU system, where multi-UAVs and targets as well as communication nodes are randomly distributed within a two dimensional area of $20 \times 20 \text{ km}^2$. Then, The main parameter settings in this paper can be seen in Table 2, which can be referred to [33,40].

Table 2. Simulation parameter settings.

Parameter	Value
Total time	$T_{\text{total}} = 600 \text{ s}$
Total power	$P_{\text{total}} = 2000 \text{ W}$
Total channel bandwidth	$B_{\text{total}} = 1000 \text{ Hz}$
Number of tasks	$N = 10$
Number of UAVs	$M = 20$
Hovering altitude of the platform in the IRCU system	$H = 500 \text{ m}$
False alarm probability	$p_{\text{fa}} = 0.0015$
Effective receiving antenna area for phased-array radars	$A_r = 0.0173 \text{ dB} \cdot \text{m}^2$
Detecting target cross area	$\sigma_d = 1 \text{ m}^2$
Tracking target cross area	$\sigma_t = 1 \text{ m}^2$
Radar constant	$L_r = 1.6 \times 10^{10}$
Channel gain of LOS	$h_0 = -20 \text{ dBm/Hz}$
Noise power spectral density	$n_0 = -169 \text{ dBm}$
The minimum power	$P_{\text{min}} = 100 \text{ W}$
The maximum power	$P_{\text{max}} = 200 \text{ W}$
UAV hovering power	$P_h = 50 \text{ W}$
The minimum bandwidth	$B_{\text{min}} = 100 \text{ Hz}$
The maximum bandwidth	$B_{\text{max}} = 300 \text{ Hz}$
The minimum task scheduling success rate	$\gamma = 0.6$
Weight coefficients	$w_1 = 0.1, w_2 = 0.6, w_3 = 0.3$
Error accuracy of LIO algorithm	$\delta = 10^{-5}$
Leaning factors of LIO algorithm	$c_1 = c_2 = c_3 = 2$

Then, we conduct simulation experiments for algorithm comparisons, i.e., the proposed algorithm and five baselines:

- Equal power and Improved PSO (PPSO): Powers of all tasks are equal, then other algorithms are the same for solving the remaining sub-problems.
- Equal channel bandwidth and SCA (BSCA): Channel bandwidths of all communication tasks are equal, then similar to the first scheme, other algorithms are also the same for solving the remaining sub-problems.
- SCA and PSO [41] (SCAP): Channel bandwidths of all communication tasks are obtained by PSO and its parameter settings can be found in [41], then the same algorithms are applied to solving the remaining sub-problems.
- SCA and GA [42] (SCAG): Channel bandwidths of all communication tasks are obtained by GA and its parameter settings can be found in [42], then the same algorithms are applied to solving the remaining sub-problems.
- SCA and Q-learning [43] (SCAQ): Channel bandwidths of all communication tasks are obtained by Q-learning and its parameter settings can be found in [43], then the same algorithms are applied to solving the remaining sub-problems.

Based on the above algorithms, various simulations were conducted by assigning reconnaissance UAVs and communication relay UAVs of the IRCU system to perform three types of tasks, i.e., the detection, tracking and communication tasks in a $20 \text{ km} \times 20 \text{ km}$ combat scenario. It is important to note that, as an integrated multi-UAV system, there is

sharing of resources, as well as resource constraints when performing multiple tasks. This requires consideration of how to schedule the various UAVs of the IRCU system so that the minimum task number requirements and the maximum system task performance are reached. And the task information can be seen in Table 3.

Table 3. Information of 10 tasks.

Task	Task Priority	Dwell Time (s)	Task Distance (km)
Detection task	1.1	3	10
Communication task	1.9	4	-
Tracking task	2.3	8	2.5
Communication task	2.5	5	-
Detection task	2.9	2	19
Tracking task	3.2	7	3.5
Tracking task	3.8	6	4.5
Communication task	4.6	4	-
Detection task	5.2	5	11
Communication task	6.0	3	-

4.1. Case

In case 1, we tested the joint performance of the IRCU system under w_j, P_{max}, B_{max} and N when using LIO algorithm, which can be seen in Figures 3–6.

Figure 3 depicts an illustration of the joint performance of LIO algorithm with different w_1, w_2 and w_3 applied to solving the considered problem. From Figure 3, we can observe that as n increases, these three curves first increase rapidly, then grow slowly and keep plateauing. By comparing the three curves with different w_1, w_2 and w_3 , we note that the maximum joint performances of the three curves do not differ significantly, while the number of iterations required to reach the maximum joint performance for the three curves is not the same. Specially, by following the order of the legend from top to bottom in the diagram, the maximum joint performance of the three curves is 116.73, 116.65 and 116.71, respectively; the number of iterations of LIO with $w_1 = 0.1, w_2 = 0.6$ and $w_3 = 0.3$ is 34, which is lowest than that of LIO with $w_1 = 0.2, w_2 = 0.4$ and $w_3 = 0.4$ and LIO with $w_1 = 0.3, w_2 = 0.5$ and $w_3 = 0.2$; the number of iterations of LIO with $w_1 = 0.3, w_2 = 0.5$ and $w_3 = 0.2$ is superior to that of LIO with $w_1 = 0.2, w_2 = 0.4$ and $w_3 = 0.4$, and their iterations are 90 and 45, respectively.

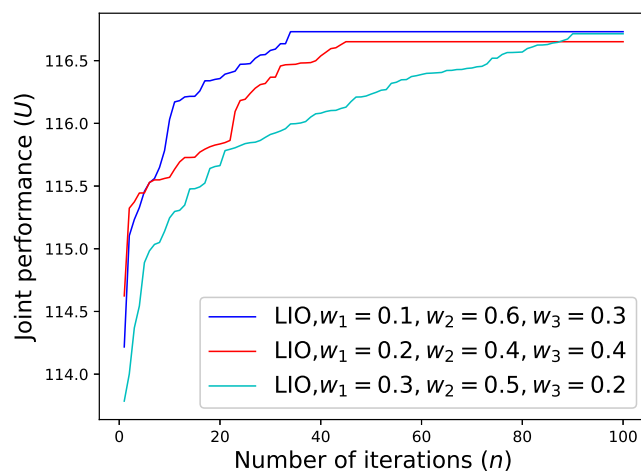


Figure 3. LIO algorithm with different w_1, w_2 and w_3 .

Figure 4 depicts an illustration of the joint performance of LIO algorithm with different P_{max} applied to solving the considered problem. In Figure 4, we can observe that as n increases, these three curves first increase rapidly, then grow slowly and keep plateauing. By comparing the three curves with different P_{max} , we note that the maximum joint

performance of LIO with $P_{\max} = 200$ W is higher than that of LIO with $P_{\max} = 150$ W and $P_{\max} = 220$ W, and the maximum joint performance of LIO with $P_{\max} = 220$ W is the lowest.

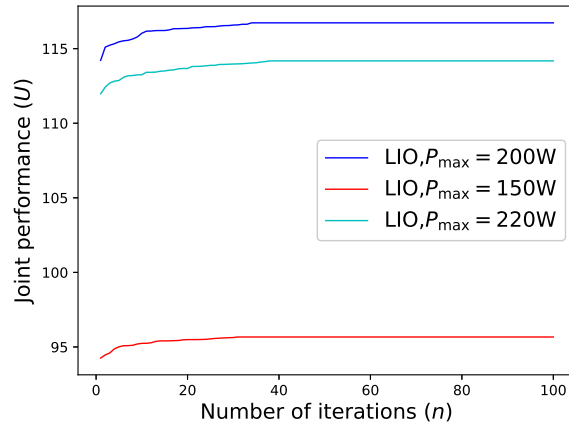


Figure 4. LIO algorithm with different P_{\max} .

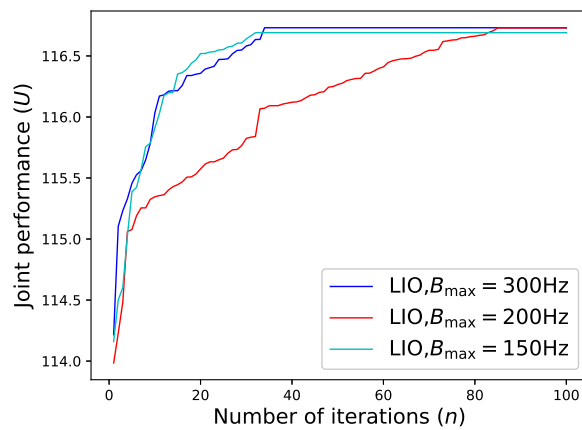


Figure 5. LIO algorithm with different B_{\max} .

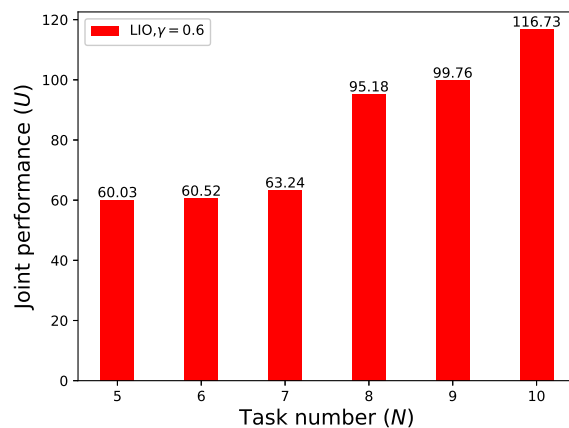


Figure 6. LIO algorithm with different N .

Figure 5 depicts an illustration of the joint performance of LIO algorithm with different B_{\max} applied to solving the considered problem. We can observe from Figure 5 that similar to the situation in Figures 3 and 4, these three curves also grow rapidly and then slowly to a plateau with the increment of n . Moreover, by comparing the three curves with different B_{\max} , we note that the maximum joint performances of the three curves do not

differ significantly, while the number of iterations required to reach the maximum joint performance for the three curves is not the same. Specially, by following the order of the legend from top to bottom in the diagram, the maximum joint performance of the three curves is 116.73, 116.73 and 116.69, respectively; the number of iterations of LIO with $B_{max} = 300$ Hz is 34, which is close to that of LIO with $B_{max} = 150$ Hz; the number of iterations of LIO with $B_{max} = 200$ Hz is the lowest, and its iterations is 85.

Figure 6 depicts an illustration of the joint performance of LIO algorithm with different N applied to solving the considered problem. We can observe from Figure 6 that with the increment of N , the joint performance increases slowly at first, and then rapidly increases when $N > 7$. Moreover, their joint performance does not differ much when N is 5, 6 and 7, respectively, which is similar to the case when N is 8 and 9. However, when N is 7 and 8, respectively, their joint performance is greatly different, which is also similar to the case when N is 9 and 10. And the reason behind this phenomenon is that the joint performance is calculated with respect to task number, weight coefficients and task scheduling success rate.

In case 2, PPSO algorithm, BSCA algorithm, SCAP algorithm, SCAG algorithm and SCAQ algorithm are both used for solving the considered problem. We compared them with LIO algorithm by obtaining the joint performance under the same system, and their joint performance changes with n in Figure 7.

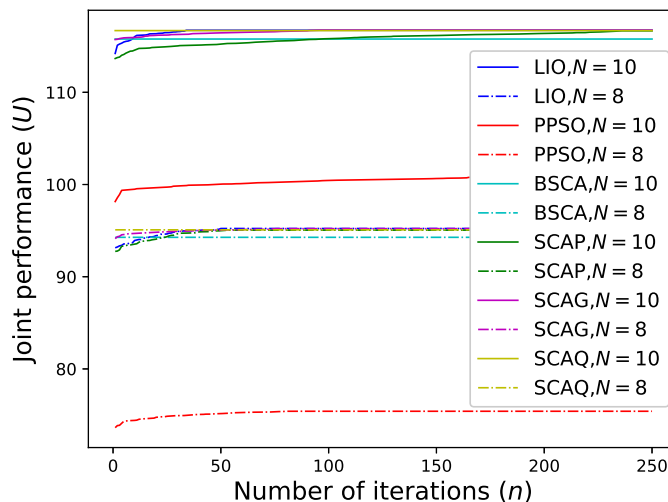


Figure 7. Comparison between different algorithms under the IRCU system.

Figure 7 depicts a comparison chart between these six algorithms applied to solving the considered problem under different numbers of tasks. When $N = 10$, we can observe that as n increases, the curve of LIO first increases rapidly, then grows slowly and remains stable when n is approximately 34. And the maximum joint performance of LIO is roughly 116.73. Similar to the curve of LIO, the curve of PPSO also grows rapidly and then slowly to a plateau when $n > 165$. But, the maximum joint performance of PPSO is inferior to that of LIO, which is roughly 100.77. Moreover, the curves of SCAP and SCAG keep growing slowly and remain steady when $n > 235$ and $n > 95$, respectively. Compared to the curve of LIO, the curves of SCAP and SCAG take more iterations to obtain the same maximum joint performance. Moreover, the curves of BSCA and SCAQ keep plateauing consistently, and their joint performance is 115.78 and 116.69, respectively. Meanwhile, the joint performance of BSCA and SCAQ is larger than that of LIO when $n < 15$ and $n < 32$, however, after $n > 15$ and $n > 32$, the situation is reversed. From Figure 7, we note that similar to the case when $N = 10$, the increasing trends of the curves when $N = 8$ also tend to be the same, except that the joint performance is lower due to the small number of tasks. The reason behind this phenomenon is that the curves of PPSO, BSCA and SCAQ do not take the optimal solution, while the curves of SCAP and SCAG converge more slowly compared to that of LIO.

4.2. Analysis

Comparing the situations of Figures 3–6, we note that w_j and B_{\max} have little impact on the maximum performance of LIO, while P_{\max} and N have a significant impact on the maximum performance of LIO. The specific reasons for these cases are as follows: when $N = 10$, $P_{\max} = 200$ W and $B_{\max} = 300$ Hz, different weight coefficients affect the proportion of each task's performance in the joint performance, but weight coefficients do not change greatly, resulting in little change in the joint performance; when $N = 10$, $P_{\max} = 200$ W, $w_1 = 0.1$, $w_2 = 0.6$ and $w_3 = 0.3$, different maximum channel bandwidths only affect the communication task, and the proportion of communication task performance in joint performance is also affected by w_3 ; when $N = 10$, $B_{\max} = 300$ Hz, $w_1 = 0.1$, $w_2 = 0.6$ and $w_3 = 0.3$, different maximum powers affect the overall tasks, leading to great change in the joint performance; when $P_{\max} = 200$ W, $B_{\max} = 300$ Hz, $w_1 = 0.1$, $w_2 = 0.6$ and $w_3 = 0.3$, different task numbers affect the overall tasks, resource allocation and task scheduling success rate, resulting in great change in the joint performance.

Comprehensively considering the situations of Figure 7, we note that the iteration number of LIO is fewer than that of PPSO, SCAP and SCAG, and the maximum joint performance of LIO is higher than that of other baseline schemes, except for SCAP and SCAG. The reason is that PPSO, BSCA and SCAQ do not take the optimal power or optimal channel bandwidth, resulting in low joint performance. Meanwhile, compared to LIO, SCAP and SCAG need more iterations in obtaining the optimal channel bandwidth, and the overall number of iterations required in obtaining the same maximum joint performance is also higher.

5. Conclusions

In this paper, the joint task allocation and resource optimization problem in the IRCU system was described and formulated, and reconnaissance UAVs and communication UAVs were considered cooperatively accomplishing the detection, tracking and communication tasks of the system under the resource, priority and timing constraints by optimizing task allocation, power as well as channel bandwidth. After that, in order to solve the complex non-convex problem, we proposed an LIO algorithm to obtain the optimal solution. In fact, the considered problem was decomposed into three sub-problems, which solved by the corresponding algorithm. Finally, simulation results verified that LIO algorithm consumes fewer iterations or gains higher maximum joint performance than other baseline schemes for solving the considered problem.

Nevertheless, there still exist challenges when applying LIO algorithm to processing the joint optimization problems, e.g., appropriate parameter settings, falling into local optimum when using the traditional intelligent algorithm, etc. In future work, we will concentrate on these problems and study the complex dynamic scenarios in an integrated multi-UAV system.

Author Contributions: Conceptualization, K.W., X.Z. and X.L.; methodology, X.Z.; software, X.Z.; validation, K.W., X.Z. and X.L.; formal analysis, K.W. and X.Z.; investigation, X.Z.; resources, Y.C.; data curation, Y.C. and K.L.; writing—original draft preparation, X.Z.; writing—review and editing, X.Z.; visualization, X.Z.; supervision, K.W.; project administration, Y.C. and K.L. All authors have read and agreed to the published version of the manuscript.

Funding: This research was funded in part by the National Natural Science Foundation of China under Grant 62172313 and 52031009, in part by the Natural Science Foundation of Hunan Province under Grant 2021JJ20054.

Data Availability Statement: Data sharing is not applied.

Conflicts of Interest: The authors declare no conflict of interest.

Appendix A

From Equations (2), (10) and (13), $R_{i,1}$, $R_{i,2}$ and $R_{i,3}$ can be sequentially written as

$$R_{i,1} = (1 + \frac{p_i A_r \sigma_d T_{c,i}}{4\pi k_B L_s T_e R_i^4 \theta}) \sqrt{p_{fa}} \tag{A1}$$

$$R_{i,2} = \frac{p_i \sigma_t L_r T_{c,i}}{R_i^4} \tag{A2}$$

$$R_{i,3} = B_i \log_2(1 + \frac{p_i h_0}{N_0 B_i}) \tag{A3}$$

Define $\alpha_1 = \frac{A_r \sigma_d T_{c,i}}{4\pi k_B L_s T_e R_i^4 \theta}$, $\alpha_2 = \frac{p_i \sigma_t L_r T_{c,i}}{R_i^4}$ and $\alpha_3 = \frac{p_i h_0}{N_0 B_i}$, and $p_{i,1}$, $p_{i,2}$ and $p_{i,3}$ are converted to

$$R_{i,1} = p_{fa}^{\frac{1}{1+\alpha_1 p_i}} \tag{A4}$$

$$R_{i,2} = \alpha_2 p_i \tag{A5}$$

$$R_{i,3} = B_i \log_2(1 + \alpha_3 p_i) \tag{A6}$$

Then, taking the second derivative for $R_{i,1}$, $R_{i,2}$ and $R_{i,3}$, respectively, we obtain

$$R''_{i,1} = [\frac{2\alpha_1^2 \ln(p_{fa})}{(1 + \alpha_1 p_i)^3} + \frac{\alpha_1^2 (\ln(p_{fa}))^2}{(1 + \alpha_1 p_i)^4}] p_{fa}^{\frac{1}{1+\alpha_1 p_i}} \tag{A7}$$

$$R''_{i,2} = 0 \tag{A8}$$

$$R''_{i,3} = -\frac{B_i \alpha_3^2}{(1 + \alpha_3 p_i)^2 \ln 2} \tag{A9}$$

According to (A7)–(A9), $R''_{i,1} > 0$, $R''_{i,2} \geq 0$, and $R''_{i,3} < 0$. Then, $R_{i,1}$, $R_{i,2}$ and $R_{i,3}$ are convex, convex and concave, respectively. Since $U(\mathbf{P})$ is the sum of $R_{i,1}$, $R_{i,2}$ and $R_{i,3}$, $U(\mathbf{P})$ is proved to be non-convex.

Thus, we successfully prove Theorem 1.

Appendix B

At the $(n + 1)$ -th iteration, given \mathbf{P}^n and \mathbf{B}^n , \mathbf{F}^{n+1} can be obtained by solving $\mathcal{P}1'$, and then we have $\mathbf{B}^{n,*}$

$$U(\mathbf{F}^{n+1}, \mathbf{P}^n, \mathbf{B}^n) \geq U(\mathbf{F}^n, \mathbf{P}^n, \mathbf{B}^n) \tag{A10}$$

Next, given \mathbf{F}^{n+1} and \mathbf{B}^n , \mathbf{P}^{n+1} can be obtained by solving $\mathcal{P}2$, then we have

$$U(\mathbf{F}^{n+1}, \mathbf{P}^{n+1}, \mathbf{B}^n) \geq U(\mathbf{F}^{n+1}, \mathbf{P}^n, \mathbf{B}^n) \tag{A11}$$

Finally, when solving the channel bandwidth sub-problem, given \mathbf{F}^{n+1} and \mathbf{P}^{n+1} , \mathbf{B}^{n+1} can be obtained by solving $\mathcal{P}3$, then we have

$$U(\mathbf{F}^{n+1}, \mathbf{P}^{n+1}, \mathbf{B}^{n+1}) \geq U(\mathbf{F}^{n+1}, \mathbf{P}^{n+1}, \mathbf{B}^n) \tag{A12}$$

As a result, we obtain at the $(n + 1)$ -th iteration

$$U(\mathbf{F}^{n+1}, \mathbf{P}^{n+1}, \mathbf{B}^{n+1}) \geq U(\mathbf{F}^n, \mathbf{P}^n, \mathbf{B}^n) \tag{A13}$$

Hence, we successfully prove Theorem 2.

References

1. Zeng, Y.; Lyu, J.; Zhang, R. Cellular-connected UAV: Potential, challenges, and Promising technologies. *IEEE Wirel. Commun.* **2019**, *26*, 120–127. [[CrossRef](#)]
2. Fotouhi, A.; Qiang, H.; Ding, M.; Hassan, M.; Giordano, L.G.; Garcia-Rodriguez, A.; Yuan, J. Survey on UAV cellular communications: Practical aspects, standardization advancements, regulation, and security challenges. *IEEE Commun. Surv. Tuts.* **2019**, *21*, 3417–3442. [[CrossRef](#)]
3. Li, B.; Fei, Z.; Zhang, Y. UAV communications for 5G and beyond: Recent advances and future trends. *IEEE Internet Things J.* **2019**, *6*, 2241–2263. [[CrossRef](#)]
4. Ryan, A.; Zennaro, M.; Howell, A.; Sengupta, R.; Hedrick, J.K. An overview of emerging results in cooperative UAV control. In Proceedings of the 2004 43rd IEEE Conference on Decision and Control (CDC), Nassau, Bahamas, 14–17 December 2004; pp. 602–607.
5. Li, B.; Fei, Z.; Dai, Y.; Zhang, Y. Secrecy-optimized resource allocation for UAV-assisted relaying networks. In Proceedings of the 2018 IEEE Global Communications Conference (GLOBECOM), Abu Dhabi, United Arab Emirates, 9–13 December 2018; pp. 1–6.
6. Xiao, Z.; Liu, D.; Fei, B.; Men, T.; Zhou, Z.; Zhang, X.; Zhou, Y. Moving Target Tracking for Single UAV In Open Outdoor Environment. In Proceedings of the 2020 6th International Conference on Big Data and Information Analytics (BigDIA), Shenzhen, China, 4–6 December 2020; pp. 317–324.
7. Wu, H.-H.; Zhou, Z.; Feng, M.; Yan, Y.; Xu, H.; Qian, L. Real-Time Single Object Detection on The UAV. In Proceedings of the 2019 International Conference on Unmanned Aircraft Systems (ICUAS), Atlanta, GA, USA, 11–14 June 2019; pp. 1013–1022.
8. Wu, Q.; Zeng, Y.; Zhang, R. Joint trajectory and communication design for multi-UAV enabled wireless networks. *IEEE Trans. Commun.* **2018**, *17*, 2109–2121. [[CrossRef](#)]
9. Ji, Y.; Dong, C.; Zhu, X.; Wu, Q. Fair-energy trajectory planning for cooperative UAVs to locate multiple targets. In Proceedings of the ICC 2019—2019 IEEE International Conference on Communications (ICC), Shanghai, China, 21–23 May 2019; pp. 1–7.
10. Do, D.T.; Le, C.B.; Vahid, A.; Mumtaz, S. Antenna selection and device grouping for spectrum-efficient UAV-assisted IoT systems. *IEEE Internet Things J.* **2023**, *10*, 8014–8030. [[CrossRef](#)]
11. Kumaravelu, V.B.; Jadhav, H.K.; Bs, A.; Gudla, V.V.; Murugadass, A.; Imoize, A.L. Unmanned Aerial Vehicle-Assisted Reconfigurable Intelligent Surface for Energy Efficient and Reliable Communication. In *Unmanned Aerial Vehicle Cellular Communications*; Springer International Publishing: Cham, Switzerland, 2023; pp. 173–201.
12. Van Nguyen, M.S.; Do, D.T.; Phan, V.D.; Ullah Khan, W.; Imoize, A.L.; Fouda, M.M. Ergodic performance analysis of double intelligent reflecting surfaces-aided NOMA-UAV systems with hardware impairment. *Drones* **2022**, *6*, 408. [[CrossRef](#)]
13. Liu, J.; Liu, Y.; Cong, M.; Wang, Z.; Wang, J. A Novel Method for Multi-UAV Cooperative Reconnaissance Mission Planning in Denied Environment. In Proceedings of the 2021 International Symposium on Computer Science and Intelligent Controls (ISCSIC), Rome, Italy, 12–24 November 2021; pp. 1–5.
14. Wang, X.; Chen, H.; Liu, T.; He, K.; Ding, D.; Yong, E. Application of Improved K-means Clustering Algorithm in UAV Reconnaissance Mission Planning. In Proceedings of the 2021 China Automation Congress (CAC), Beijing, China, 22–24 October 2021; pp. 2744–2748.
15. Wu, Y.; Low, K.H.; Lv, C. Cooperative Path Planning for Heterogeneous Unmanned Vehicles in a Search-and-Track Mission Aiming at an Underwater Target. *IEEE Trans. Veh. Technol.* **2020**, *69*, 6782–6787. [[CrossRef](#)]
16. Zhang, K.; Li, Z.; Zhao, X.; Zhao, B. Dynamic Multi-UAV Cooperative Reconnaissance Task Assignment Based on ICNP. In Proceedings of the 2020 5th International Conference on Mechanical, Control and Computer Engineering (ICMCCE), Harbin, China, 25–27 December 2020; pp. 773–779.
17. Xia, Z.; Du, J.; Jiang, C.; Wang, J.; Ren, Y.; Li, G. Multi-UAV Cooperative Target Tracking Based on Swarm Intelligence. In Proceedings of the ICC 2021—IEEE International Conference on Communications, Montreal, QC, Canada, 14–23 June 2021; pp. 1–6.
18. Gao, S.; Zuo, L.; Bao, S.X. UAV Reconnaissance Task Allocation with Reinforcement Learning and Genetic Algorithm. In Proceedings of the 2022 International Conference on Automation, Robotics and Computer Engineering (ICARCE), Wuhan, China, 14–16 December 2022; pp. 1–3.
19. Pitre, R.R.; Li, X.R.; Delbalzo, R. UAV Route Planning for Joint Search and Track Missions—An Information-Value Approach. *IEEE Trans. Aerosp. Electron. Syst.* **2012**, *48*, 2551–2565. [[CrossRef](#)]
20. Hassanien, A.; Amin, M.G.; Zhang, Y.D.; Ahmad, F. Dual-function radar-communications: Information embedding using sidelobe control and waveform diversity. *IEEE Trans. Signal Process.* **2016**, *64*, 2168–2181. [[CrossRef](#)]
21. Liu, F.; Zhou, L.; Masouros, C.; Li, A.; Luo, W.; Petropulu, A. Toward dual-functional radar-communication systems: Optimal waveform design. *IEEE Trans. Signal Process.* **2018**, *66*, 4264–4279. [[CrossRef](#)]
22. Liu, F.; Zhou, L.; Masouros, C.; Li, A.; Luo, W.; Petropulu, A. Dual-functional cellular and radar transmission: Beyond coexistence. In Proceedings of the 2018 IEEE 19th International Workshop on Signal Processing Advances in Wireless Communications (SPAWC), Kalamata, Greece, 25–28 June 2018; pp. 1–5.
23. Liu, F.; Masouros, C.; Li, A.; Sun, H.; Hanzo, L. MU-MIMO communications with MIMO radar: From co-existence to joint transmission. *IEEE Trans. Wirel. Commun.* **2018**, *17*, 2755–2770. [[CrossRef](#)]
24. Sturm, C.; Zwick, T.; Wiesbeck, W. An OFDM system concept for joint radar and communications operations. In Proceedings of the VTC Spring 2009—IEEE 69th Vehicular Technology Conference, Barcelona, Spain, 26–29 April 2009; pp. 1–5.

25. Zhang, J.A.; Huang, X.; Guo, Y.J.; Yuan, J.; Heath, R.W. Multibeam for joint communication and radar sensing using steerable analog antenna arrays. *IEEE Trans. Veh. Technol.* **2019**, *68*, 671–685. [\[CrossRef\]](#)
26. Luo, Y.; Zhang, J.A.; Ni, W.; Pan, J.; Huang, X. Constrained multibeam optimization for joint communication and radio sensing. In Proceedings of the 2019 IEEE Global Communications Conference (GLOBECOM), Waikoloa, HI, USA, 9–13 December 2019; pp. 1–6.
27. Xu, X.; Tao, R.; Li, S.; Chen, Y. Collaborative UAV Deployment and Task Allocation for Environment Sensing in Multi-UAV Networks. In Proceedings of the 2022 IEEE International Conference on Unmanned Systems (ICUS), Guangzhou, China, 28–30 October 2022; pp. 738–743.
28. Zhou, L.; Leng, S.; Wang, Q.; Liu, Q. Integrated Sensing and Communication in UAV Swarms for Cooperative Multiple Targets Tracking. *IEEE Trans. Mob. Comput.* **2022**, *in press*. [\[CrossRef\]](#)
29. Meng, K.; He, X.; Wu, Q.; Li, D. Multi-UAV Collaborative Sensing and Communication: Joint Task Allocation and Power Optimization. *IEEE Trans. Wirel. Commun.* **2023**, *22*, 4232–4246. [\[CrossRef\]](#)
30. Meng, K.; He, X.; Wu, Q.; Li, D. Multi-UAV Cooperative Sensing and Communication with Replicated Task Allocation. In Proceedings of the 2022 IEEE Globecom Workshops (GC Wkshps), Rio de Janeiro, Brazil, 4–8 December 2022; pp. 910–915.
31. Hou, D.; Qi, F.; Dai, J.; Yang, Z. Models for Radar Detection Probability Based on Operation Simulation. *Electron. Inf. Warf. Technol.* **2016**, *31*, 61–64.
32. Yan, J.; Pu, W.; Dai, J.; Liu, H.; Bao, Z. Resource Allocation for Search and Track Application in Phased Array Radar Based on Pareto Bi-Objective Optimization. *IEEE Trans. Veh. Technol.* **2019**, *68*, 3487–3499. [\[CrossRef\]](#)
33. Mynar, Z.; Vaclavek, P.; Blaha, P. Synchronous Reluctance Motor Parameter and State Estimation Using Extended Kalman Filter and Current Derivative Measurement. *IEEE Trans. Ind. Electron.* **2021**, *68*, 1972–1981. [\[CrossRef\]](#)
34. Li, X.; Yao, H.; Wang, J.; Xu, X.; Jiang, C.; Hanzo, L. A Near-Optimal UAV-Aided Radio Coverage Strategy for Dense Urban Areas. *IEEE Trans. Veh. Technol.* **2019**, *68*, 9098–9109. [\[CrossRef\]](#)
35. Chen, J.; Wu, Q.; Xu, Y.; Qi, N.; Guan, X.; Zhang, Y.; Xue, Z. Joint Task Assignment and Spectrum Allocation in Heterogeneous UAV Communication Networks: A Coalition Formation Game-Theoretic Approach. *IEEE Trans. Wirel. Commun.* **2021**, *20*, 440–452. [\[CrossRef\]](#)
36. Smith, E.; Trefftz, C.; DeVries, B. A Divide-and-Conquer Algorithm for Computing Voronoi Diagrams. In Proceedings of the 2020 IEEE International Conference on Electro Information Technology (EIT), Chicago, IL, USA, 31 July–1 August 2020; pp. 495–499.
37. Razaviyayn, M.; Hong, M.; Luo, Z.-Q.; Pang, J.-S. Parallel successive convex approximation for nonsmooth nonconvex optimization. In Proceedings of the 27th International Conference on Neural Information Processing Systems—Volume 1 (NIPS’14), Montreal, QC, Canada, 8–13 December 2014; MIT Press: Cambridge, MA, USA, 2014; pp. 1440–1448.
38. Grant, M.; Boyd, S.; Ye, Y. *CVX: Matlab Software for Disciplined Convex Programming*; CVX Research, Inc.: Austin, TX, USA, 2008.
39. Li, Y.; Long, X.; Liu, X. Mission Arrangement Optimization with Improved PSO for Multiple Plant Protection UAVs in Heterogeneous Farmlands. In Proceedings of the 2021 China Automation Congress (CAC), Beijing, China, 22–24 October 2021; pp. 7772–7776.
40. Fan, S.; Wang, Y.; Tian, H.; Jie, Z.; Shi, J. Joint Task optimization of trajectory and resource allocation for UAV integrated radar and communication system. *IEEE J. Commun.* **2021**, *42*, 182–192.
41. Sarfo, K.; Wang, K.; Rakotomandimby F., M.; Ntiamoah-Sarpong, K. Large-scale UAV-Network using the Hata—Okumura model with PSO algorithm for Open Area Communication. In Proceedings of the 2021 International Conference on Computer Engineering and Artificial Intelligence (ICCEAI), Shanghai, China, 27–29 August 2021; pp. 138–142.
42. Wu, X.; Yin, Y.; Xu, L.; Wu, X.; Meng, F.; Zhen, R. Multi-UAV Task Allocation Based on Improved Genetic Algorithm. *IEEE Access* **2021**, *9*, 100369–100379. [\[CrossRef\]](#)
43. Jones, M.R.; Djahel, S.; Welsh, K. MQTPP—Towards Multiple Q-Table based Path Planning in UAV Environments. In Proceedings of the 2022 IEEE 19th Annual Consumer Communications and Networking Conference (CCNC), Las Vegas, NV, USA, 8–11 January 2022; pp. 457–460.

Disclaimer/Publisher’s Note: The statements, opinions and data contained in all publications are solely those of the individual author(s) and contributor(s) and not of MDPI and/or the editor(s). MDPI and/or the editor(s) disclaim responsibility for any injury to people or property resulting from any ideas, methods, instructions or products referred to in the content.